Mg-Modified Sugarcane Bagasse Biochar for Dual Removal of Ammonium and Phosphate Ions from Aqueous Solutions

Maher E. Saleh[1] and Ramzy M. R. Hedia[1]

ABSTRACT

Utilization of agricultural wastes to generate cheap and efficient sorbents to remove contaminants from wastewaters is an up-to-date environmental challenge. In Egypt, sugarcane bagasse is yearly generated as a waste material in huge amounts. The objectives of this study were to investigate the effect of chemical modification on the properties of bagasse biochar generated from local sugarcane bagasse feedstock (SCBF) and assess its efficiency for removal of both ammonium and phosphate ions from artificial aqueous solutions. SCBB and Mg-SCBB biochars were produced through pyrolysis of raw SCBF and MgSO$_4$ impregnated SCBF, respectively at 500 ◦C and under oxygen-limited condition. FTIR peaks analysis, DEM examination, and some physical and chemical properties revealed that new surface functional groups, meso- and micropores, larger surface area and higher CEC were developed in SCBB and Mg-SCBB compared to SCBF. SCBB and Mg-SCBB showed high affinity to ammonium adsorption from aqueous solutions comparable to Charcoal and Zeolite. Mg-SCBB was the only sorbent capable of removing phosphate from the aqueous. Ammonium and phosphate removal at 1:200 sorbent to solution ratio were higher than those at 1:500 for all sorbents. A slight ammonium volatilization occurred during the adsorption process due to high solution pH. Adsorption kinetics data were best fitted to the pseudo-second-order kinetic equation suggesting intraparticle diffusion controlled adsorption process. Ammonium adsorption isotherms were best fitted to Freundlich model. The calculated Freundlich intensity parameter (*n*) ranged from 0.478 to 0.894 indicating favorable adsorption of ammonium and phosphate by all sorbents. Mg-SCBB had an adsorption capacity of 2573.9 and 4002.2 mg kg^{-1} for ammonium and phosphate, respectively. The produced Mg-modified sugarcane bagasse biochar may represent a promising efficient and cheap sorbent for dual remediation of wastewaters contaminated with ammonium and phosphate ions.

Keywords: Sugarcane bagasse, Mg-modified biochar, ammonium and phosphate removal, agricultural wastes, aqueous solutions.

INTRODUCTION

Due to fast industrialization and the widespread application of agrochemicals, the occurrence of organic and inorganic pollutants has considerably increased in our environment and food chain. Therefore, serious public and governmental concerns about the environmental pollution and human health have been raised (WHO, 2017). Due to inefficient management of agricultural fertilizers and large discharge of wastewaters, the concentrations of various nutrients (NH$_4^+$, NO$_3^-$ and PO$_4^{-3}$) are largely increased in surface and groundwater resources globally (Carey *et al.*, 2015). Freshwater containing elevated nutrients concentrations discharges into oceans depleting dissolved oxygen concentrations and promoting harmful algal blooms. This creates hypoxic 'dead zones' and causes ecological damage (Dunnivant and Anders, 2006).

Ammonium ion has a positive charge and a much lower charge-to-radius ratio than many metal cations. Therefore, NH$_4^+$ is mainly attracted to the negatively charged surfaces of colloidal particles and behaves similarly to alkali metal cations (e.g. Na$^+$, K$^+$). Unlike divalent metal cations, NH$_4^+$ does not form stable bonds with surfaces to which it is attached. However, the oxyanions NO$_3^-$ and PO$_4^{-3}$ are negatively charged and thus attracted to positively charged surfaces. With different behavior to each other, NO$_3^-$ is much more mobile while PO$_4^{-3}$ is readily bound to surfaces of colloidal particles in water (Conley *et al.*, 2009). Common methods of remediation polluted aqueous phases include ion exchange, precipitation, membrane separation and adsorption (using activated carbon) techniques among others. These techniques are expensive and produce chemical residues which have uneconomic value.

Biochar is a carbonaceous, fine-grained, porous solid material produced by pyrolysis of a wide variety of biomasses under different conditions. As a low-cost substitute of activated carbon, biochar can be used as carbon sequestration and soil amendment (Carey *et al.*, 2015; Agegnehu *et al.*, 2017). Besides, biochar is recently used as a green environmental sorbent to remove diverse organic contaminants such as aromatic dyes, antibiotics, polychlorinated biphenyls (PCBs), polycyclic aromatic hydrocarbons (PAHs), volatile organic compounds (VOCs) and agrochemicals from aqueous and gaseous phases (Qiu *et al.*, 2009; Beesley *et al.*, 2010; Zheng *et al.*, 2010; Teixido *et al.*, 2011; Xu *et al.*, 2011; Saleh *et al.*, 2016; De Jesus *et al.*, 2017), or inorganic contaminants such as heavy metals and various nutritional elements (NH$_4^+$, NO$_3^-$ and PO$_4^{-3}$) from urban and industrial wastewaters and agricultural drainage water (Fang *et al.*, 2014; Saleh *et al.*, 2012;

Saleh *et al.*, 2013; Hafshejani *et al.*, 2016; Cai *et al.*, 2017; Strock *et al.*, 2017). Biochar has been recently used to improve agricultural ecosystems and reduce the emission of greenhouse gases (Ulyett *et al.*, 2014; Tan *et al.*, 2017). Biomass is converted to biochar by pyrolysis, a thermochemical process under oxygen-limited or anoxic conditions (Zhang *et al.*, 2010). The conversion process includes drying and grinding of biomass, pyrolysis and then separation (Pan *et al.*, 2010). Factors affecting the characteristics of generated biochar include the type of feedstock, reaction time and conditions of thermochemical conversion (Zhang *et al.*, 2015; Li *et al.* 2016; Sizmur *et al.*, 2017; Tan *et al.* 2017). While the alkaline nature of biochar is determined by the metal alkalinity content of ash, cation exchange capacity is related to the surface area, surface functional groups (mainly carboxyl groups), type of feedstock and temperature of pyrolysis (Jiang *et al.*, 2013; Luo *et al.*, 2015; El-Gamal *et al.*, 2017).

Sugar production in Egypt is expected to reach 2.42 MMT (Million Metric Tons) in 2017/2018. About 42% of this production (1.02 MMT) is produced from sugarcane (FAS-USDA, 2017). Sugarcane is also a source of molasses. In this report, sugarcane cultivated area was forecasted to increase 10,000 ha to reach 119,000 ha in 2017/18, mostly located in Upper Egypt. Bagasse, as the residue of sugarcane processing, is limitedly used in paper pulp and plywood industries. Therefore, a large amount of sugarcane bagasse is not economically utilized. Several attempts have been made to increase the value of sugarcane bagasse through conversion to biochar by pyrolysis (Hugo, 2010; Jeong *et al.*, 2016). Sugarcane bagasse biochar (SCBB) was produced under various pyrolysis conditions (Ding *et al.*, 2014; Cha *et al.*, 2016; Huang *et al.*, 2015; Li *et al.*, 2016) including temperature (ranged from 250 to <900 ∘C) which affects its porosity and specific surface area (SSA), heating facilities (traditional kilns, muffle furnace, or microwave oven), reaction time (ranged from 20 min to 8 h) and atmosphere (oxygen-limited, vacuum or N_2-saturated atmosphere). Sugarcane bagasse was used either in its raw state (Hugo, 2010; Ding *et al.*, 2014; Jeong *et al.*, 2016), anaerobically digested (Inyang *et al.*, 2010), or subjected to different physical or chemical treatments to enhance its sorption capacity and/or selectivity (Hafshejani *et al.*, 2016; Noraini *et al.*, 2016; Schwantes *et al.*, 2015).

The efficiency of SCBB was investigated to remove heavy metals such as cadmium, chromium, lead and mercury (Ding *et al.*, 2014; Li *et al.*, 2017; Noraini *et al.*, 2016), organic dyes (Carrier *et al.*, 2012), nitrate (Schwantes 2015; Hafshejani *et al.*, 2016) and phosphate (Trazzi *et al.*, 2016) from aqueous solutions or wastewaters.

Ding *et al.* (2014) found that SCBB produced at different pyrolysis temperatures (from 250 to 600 ∘C) was effective in Pb^{2+} sorption from aqueous solutions and the sorption capacity of the produced biochar decreased with increasing the temperature of pyrolysis (from 2.1 to 6.1 mg Pb/g biochar at 250 and 600 ∘C, respectively). The initially, rapid Pb sorption was probably controlled by ion exchange and/or complexation then it was slowed down due to intraparticle diffusion. Noraini *et al.*, (2016) reported that magnetic biochar produced from sugarcane bagasse by microwave heating at optimum conditions of 30 min of radiation time and Fe_2O_3 impregnation ratio 0.45 (Fe_2O_3 : biomass), could enhance the removal efficiency of Cd^{2+} to 96.17% from aqueous solutions. Carrier *et al.* (2012) obtained a high-quality SCBB was also produced by vacuum pyrolysis and steam activation having an SSA of 418 m^2 g^{-1} and a cation exchange capacity (CEC) of 122 $cmol_c$ kg^{-1}. This biochar was very efficient in methylene blue (MB) adsorption and favored physisorption rather than chemisorption.

The efficiency of nitrate adsorption by SCBB, generated at 300 ∘C for 4 h in a carbonization furnace, was enhanced by chemical modification of air-dried bagasse using epichlorohydrin, dimethylformamide and ethylenediamine combination before pyrolysis (Hafshejani *et al.*, 2016). Adsorption capacity for nitrate removal from aqueous solutions was increased from 11.56 to 28.21 mg g^{-1} for SCBB and modified SCBB, respectively. The maximum capacity (q_{max}) of nitrate was reached with sorbent dose of 2 g L^{-1}, equilibrium pH 4.64 and after 60 min of contact time. Schwantes *et al.* (2015) showed that SCBB produced from 3 *M* H_3PO_4-activated bagasse was efficient in NO_3^- removal from aqueous solutions. The adsorption isotherms followed the Freundlich model and sorption kinetics data were fitted to the pseudo-second-order equation.

Trazzi *et al.* (2016) found that surface area and fixed carbon content of SCBB were increased with increasing pyrolysis temperature and residence time. The best performance was observed for SCBB formed at 500 ∘C for 60 min. in terms of energy expended and phosphate sorption. Adsorption on of phosphate was found to be non-spontaneous, endothermic process and adsorption capacity increased with temperature.

Therefore, the objectives of this study were to investigate the effect of chemical modification on the properties of bagasse biochar generated from local sugarcane bagasse and to assess its efficiency for removal of both ammonium and phosphate ions from aqueous solutions.

MATERIALS AND METHODS

Preparation of feedstock:

Sugarcane bagasse feedstock (SCBF) was collected from the local market in Alexandria Governorate. SCBF was cut into 2.0 cm segments, washed with tap water, then with distilled water and oven-dried at 70 ◦C for 24 h. The oven-dried SCBF was left to cool to reach the ambient lab temperature and then stored in a plastic vessel for the pyrolysis step. A slight modification to the method outlined by Fang et al. (2014) was made to prepare Mg-saturated SCBF. A portion of the oven-dried SCBF was soaked in 1.6 M $MgSO_4.7H_2O$ at 1:10 solid to solution ratio for 2 h. The Mg-saturated SCBF (Mg-SCBF) was then oven-dried at 80 ◦C for 48 h, left to cool to ambient temperature and stored in a plastic vessel for the pyrolysis step.

Generation of biochar:

Biochar was generated by heating SCBF and Mg-SCBF under oxygen-limited condition (pyrolysis). For pyrolysis, 200 g of both previously prepared SCBF and Mg-SCBF was tightly wrapped in an aluminum foil sheet. The wrappings were perforated with five tiny halls to allow pyrolytic gases to escape and facilitate an oxygen-limited condition. Pyrolysis was conducted in a muffle furnace by increasing temperature at a rate of 25 ◦C/min to reach 500 ◦C and then heating was continued at 500 ◦C for 60 min. The generated bagasse (SCBB) and the Mg-modified bagasse biochars (Mg-SCBB) were left to cool to room temperature and the produced carbonaceous material was weighed. Afterwards, biochars were ground in a porcelain mortar and pestle and sieved through 0.5 mm polyethylene sieve. The biochars were then washed several times with distilled water, oven-dried at 80 ◦C for 24 h, left to cool to room temperature and finally stored in plastic vessels for subsequent experiments.

Characterization of sorbents:

Percent of biochar yield and volatile matter were calculated from the oven-dried SCBF and the generated carbonized materials after pyrolysis. The pH was measured (pH-meter, Inolab pH/Ion 735) in the suspensions of 1.0 g biochar in 100 ml of distilled water. The electrical conductivity (EC, dS m^{-1}) was measured using a conductivity meter (WTW inoLab Cond 720, GmbH) in the filtrate of a 5% W/V solid/distilled water suspension. Surface area (m^2 g^{-1}) of the biochars was determined using the methylene blue method (Kaewprasit et al., 1998). The ash content of biochars was determined according to Samsuri et al. (2014) in open porcelain crucibles using the muffle furnace at 700 ◦C for 12 hrs. Cation exchange capacity (CEC) was determined using the modified ammonium acetate compulsory displacement procedure (Gaskin et al., 2008). The CHNS Elemental Analyzer (Vario, type El) was utilized to determine the carbon, hydrogen, nitrogen, and sulfur contents.

Fourier transform infrared (FTIR) spectra of the biochars and bagasse feedstock were established in the range 400–4000 cm^{-1} (SHIMADZU infrared spectrophotometer; model FT/IR-5300, JASCO Corporation) to determine predominant surface functional groups. Images of a scanning electron microscope (SEM, Jeol model 6360 OLA) was used to investigate the surface micro-morphology of biochars.

For comparison, Zeolite and Charcoal, as commercial adsorbents, were purchased from private companies to be used for the comparison with the generated biochars for their efficiencies of ammonium and phosphate ions removal from aqueous solutions.

Stock solution of ammonium and phosphate:

A stock solution containing 500 mg P/l and 580 mg NH_4^+/l was prepared using an analytical grade of di-ammonium orthophosphate salt (2.129 g $(NH_4)_2HPO_4$/l). From the stock solution, aqueous solutions with a series of NH_4^+ and P concentrations were prepared for the proposed adsorption experiments.

Kinetics of ammonium and phosphate sorption:

The kinetics of ammonium and phosphate removal by the four sorbents (SCBB, Mg-SCBB, Zeolite, and Charcoal) from aqueous solutions was investigated using the compartment method. Artificial aqueous solutions containing 23.2 ppm NH_4^+ and 20 ppm P (representing average concentrations of such species in local municipal wastewater) were prepared from the stock solution. In a double jacket reaction vessel (Fig. 1), 2 or 5 g of each sorbent was suspended in 1000 ml aqueous solution to represent 1:200 or 1:500 sorbent to solution ratio. The reaction took place in the inner vessel. The suspension was continuously stirred at 500 rpm using magnetic stirrer and temperature of the suspension was kept constant at 25◦C using a continuous circulating thermostatic water system running in the outer vessel and surrounding the reaction inner vessel. Subsamples of suspension (20 ml) were withdrawn from the reaction vessel using a manual syringe at time intervals of 1, 2, 3, 4, 6, 8, 10, 12 and 24 h and pH of the sampled suspensions was immediately measured. The suspensions were then filtered through a filter paper (Whatman no. 1) and the equilibrium concentrations of ammonium and phosphate were measured in the filtrates. The concentrations of ammonium and phosphate were determined colorimetrically according to the methods described by Keeney and Nelson (1982) and Murphy and Riley (1962), respectively.
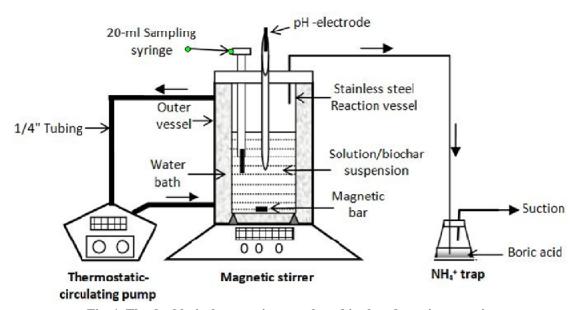
Fig. 1. The double-jacket reaction vessel used in the adsorption experiments

The amount of ammonium and phosphate adsorbed per sorbent unit mass (q, mg g^{-1}) were calculated using equation (1).

$$q = \frac{(C_o - C_{eq})}{m} v \qquad (1)$$

Where C_0 and C_{eq} are the initial and equilibrium concentrations (mg/l), respectively, m is the mass of sorbent material (g), and v is the volume of aqueous solution (l).

For correction of ammonia volatilization, the evolved ammonia from the reaction vessel at each time interval was collected and trapped in 25 ml of boric acid for its measurement. Plots of sorption kinetics (time vs. q) were established and the equilibrium time was evaluated. The fitness of these plots to the first- and second-order mathematical models of reaction kinetics was also investigated.

The removal percentage of adsorbate (R, %) was also calculated from Equation (2) as follows;

$$R\% = \frac{(C_0 - C_{eq})}{C_0} \times 100 \qquad (2)$$

Isotherms of ammonium and phosphate sorption:

Sorption isotherms of NH_4^+ and P on the investigated sorbents were established using the 1:200 and 1:500 suspension ratios and a series of initial concentrations of NH_4^+ (23.2, 46.4 and 92.6 ppm) and P (20, 40 and 80 ppm). The sorption reaction was conducted for each individual sorbent under the same conditions of the aforementioned kinetic experiment (stirring at 500 rpm and temperature at 25 °C).

Suspensions were sampled at the equilibrium time determined from the kinetic experiment. Similarly, pH was measured immediately in the suspension and NH_4^+ and P were also measured in the filtrate using the same methods. Ammonia volatilization was also determined for the correction of sorbed NH_4^+. Sorption isotherms were plotted (q vs. C_{eq}) and the fitness to Freundlich and Langmuir adsorption mathematical models were tested.

Mathematical Models

Kinetic models:

The model expressed in Equation (3) was used to describe the intra-particle diffusion as the controlling step for the adsorption process (Weber and Morris, 1963; Zhang et al., 2015).

$$q_t = K_p t^{1/2} + C \qquad (3)$$

Where k_p is the rate constant of intra-particle diffusion (mg/g.min$^{1/2}$), and C (mg/g) is the intercept. A linear plot of q_t against $t^{1/2}$ can be used to test the goodness-of-fit of the experimental data to the pseudo-first-order model.

The Lagergren pseudo-first-order kinetic model can be expressed by Equation (4)

$$\frac{dq_t}{dt} = k_1(q_e - q_t) \qquad (4)$$

Where k_1 is the adsorption rate constant (g/min), q_e is the amount of phosphate adsorbed at equilibrium (mg/g), and q_t is the amount of adsorbed phosphate at time t (mg/g). For limits of the initial conditions from

$q_t= 0$, at t= 0 to $q_t =q_t$ at time t, the integration of Equation (5) yields:

$$q_t = q_e[1 - \exp(-k_1 t)] \qquad (5)$$

The linearized form of this integral can be expressed in Equation (6);

$$\ln(q_t - q_e) = \ln q_e + k_1 t \qquad (6)$$

Where q_e and k_1 can be obtained from the regression plot of $\ln(q_t-q_e)$ against t.

The pseudo-second-order model (Ho and McKay, 1999; Ho, 2006) can be expressed by Equation (7):

$$\frac{dq_t}{dt} = k_2 (q_e - q_t)^2 \qquad (7)$$

The integration of the of Equation (7) for the initial conditions $q_t= 0$ at t= 0 yields

$$q_t = \frac{q_e^2 k_2 t}{1+q_e k_2 t} \qquad (8)$$

Where k_2 is the adsorption rate constant (g/mg min), q_e is the amount of adsorbed phosphate (mg/g) at equilibrium, and q_t is the amount of adsorbed phosphate at time t (mg/g).

The linearization of Equation (8) was developed in different versions (Ho, 2006; Ghasemi et al., 2013; Plazinski et al., 2013) as presented in Table (1).

Table 1. Different versions of pseudo-second-order model used for adsorption kinetics studies

Linearized versions	Equation No.
$\dfrac{t}{q} = \dfrac{1}{kq_e^2} + \dfrac{1}{q_e}t$	$8-1$
$\dfrac{1}{q} = \dfrac{1}{q_e} + \left(\dfrac{1}{kq_e^2}\right) + \dfrac{1}{t}$	$8-2$
$q = q_e - \left(\dfrac{1}{kq_e}\right)\dfrac{q}{t}$	$8-3$
$\dfrac{q}{t} = kq_e^2 - kq_e q$	$8-4$

Models for sorption isotherms:

The empirical Freundlich linearized model expressed in Equation (9) was used to describe the relation between the amount of adsorbed ammonium or phosphate (q_e) on biochar and their concentration (C_e) at equilibrium.

$$\log q_e = \log k_f + \frac{1}{n}\log C_e \qquad (9)$$

Where K_f and $1/n$ are the constants that reflect the capacity and intensity of adsorption. These constants

can be calculated from the plots of log q_e against log C_e, were $1/n$ equals the slope of the straight line and K_f equals its intercept.

Also, the commonly applied Langmuir linearized model is expressed in Equation (10).

$$\frac{C_e}{q_e} = \frac{C_e}{q_{max}} + \frac{1}{q_{max} K_1} \qquad (10)$$

Where q_{max} is the maximum monolayer adsorption capacity (mg kg^{-1}) and K_L is a constant that reflects the favorability of the adsorption process. The plots of C_e/q_e against C_e give a straight line whose slope equals $1/q_{max}$ and the intercept equals $1/q_{max} K_L$.

Data of the sorption kinetics experiments were analyzed to find the most successful mathematical model to describe the removal of ammonium and phosphate by the generated sugarcane bagasse biochars. The least squared differences technique was applied and the Coefficient of determination (R^2) was used as the statistical criteria for the goodness-of-fit of the tested models to the experimental data.

RESULTS AND DISCUSSION

Characteristics of generated biochars:

Physical characteristics:

When 200 g of sugarcane bagasse feedstock (SCBF) was soaked in the MgSO$_4$ solution and then dried at 80∘C, the final weight obtained was 302.82 g. The percent increase in the Mg-impregnated feedstock was 54.41% and it was due to the absorbed amount of MgSO$_4$ salt within the capillary tissue of the sugarcane bagasse. After pyrolysis at 500 ∘C, 51.16 and 105.93 g of SCBB and Mg-SCBB were obtained, respectively. Thus, the calculated biochar yields from feedstock were 25.58 and 34.98 % on the dried mass basis (Table 2). This was due to dehydration and condensation processes. Volatile matter contents were calculated to be 74.42 and 65.02 % for SCBB and Mg-SCBB, respectively. SCBB ash and moisture contents were lower than those of Mg-SCBB due to the higher Mg content of the latter. The generated SCBB biochar had a black color and Mg-SCBB had a dark gray color and higher ash content due also to its high Mg content.

Chemical characteristics:

The generated SCBB and Mg-SCBB had higher pH values than SCBF (Table 2) and Mg-SCBB was more alkaline than SCBB. In addition, the EC values (dS m^{-1}) of SCBB and Mg-SCBB were slightly higher compared to its value for SCBF feedstock (Table 2). Carbon, hydrogen, nitrogen, and sulfur contents of biochars were higher than the bagasse feedstock due to condensation and they were comparable to those

Table 2.Main physical and chemical characteristics of sugarcane bagasse feedstock and the tested sorbents

Criteria	SCBF Feedstock	Biochars		Charcoal	Zeolite
		SCBB	Mg-SCBB		
Physical characteristics					
Biochar yield, %	-	25.58	34.98	-	-
Volatile matter, %	-	74.42	65.02	-	-
Ash, %	-	15.61	20.64	-	-
Color	-	black	dark gray	black	white
Surface area, $m^2\ g^{-1}$	-	38.74	42.12	35.61	49.87
Chemical characteristics					
EC, $dS\ m^{-1}$	0.70	0.95	1.02	0.87	0.74
pH	3.36	7.09	9.88	8.95	6.95
CEC, $cmol\ kg^{-1}$	-	34.74	39.57	31.24	48.02
C, %	42.82	67.61	64.35	65.84	-
N, %	0.55	0.79	0.73	0.76	-
C/N ratio	77.85	85.6	88.2	86.63	-
S, %	0.42	0.39	0.34	0.41	-

obtained by many researchers (Saleh et al., 2013; Jindo *et al.,* 2014; El-Gamal et al., 2017). The elemental contents for Mg-

SCBB were slightly lower compared to SCBB presumably due to its higher Mg content. Condensation led also to the increase in the C/N ratio from 77.85 for bagasse feedstock to 85.6 and 88.2 for SCBB and Mg-SCBB, respectively. Sulfur content was slightly reduced after pyrolysis (Table 2).

Surface functional groups by FTIR analysis:

The FTIR spectra of SCB feedstock and the generated biochars SCBB and Mg-SCBB are presented in Fig. (2). Generally, the peaks obtained for the three materials are different in their wave numbers peaks and intensities. Peaks of O-H stretching of free hydroxyl group were observed within the range from 3813.4 and 3786.39 cm^{-1}, from 3875.12 to 3757.46 cm^{-1}, and from 3861.62 to 3734.31 cm^{-1}, for SCBF, SCBB, and Mg-SCBB, respectively indicating the chemically adsorbed water molecules and surface hydroxyl groups. SCBF had the highest intensity of free OH peaks and it was much lesser in SCBB and Mg-SCBB (Saleh et al., 2013). This may indicate the loss of free water molecules from SCBF during the pyrolysis process at 500 °C.

The presence of OH groups and H-bonds bands of alcohols and phenols were observed at peaks 3410.26, 3446.91, and 3396.76 cm^{-1} for SCBF, SCBB, and Mg-SCBB, respectively (Jindo et al., 2014). The intensities of these peaks were the highest for Mg-SCBB (Daffalla et al., 2010). This may be due to the initial impregnation of SCBF with a MgSO₄ solution, heating at 105 and the formation of MgO due to SO_2 gas evolution and the formation of a surface precipitate of metal oxide and

hydroxide surfaces (Claoston et al., 2014; Sizmur et al., 2017).

Peaks assigned to aliphatic C-H vibrational stretching appeared in SCBF spectrum at 2921.61 cm^{-1} indicating the presence of alkanes. However, this peak was not detected in SCBB or in Mg-SCBB spectra. This may indicate dehydration of cellulosic and ligneous components and thus the dehydrogenation of methylene groups of bagasse feedstock which led to a condensed structure of the generated biochars. Peaks of stretching C≡C existed in SCBF, SCBB, and Mg-SCBB spectra at 2142.99, 2357.09, and 2349.38 cm^{-1}, respectively, with descending intensity in the order:Mg-SCBB> SCBB > SCBF which is consistent with increasing the degree of condensation due to pyrolysis. Peaks at 1633.76, 1583.61, and 1660.77 cm^{-1} assigned to C=O groups stretching were detected in SCBF, SCBB, and Mg-SCBB (Harvey et al., 2012; Saleh et al., 2013 and Yao et al., 2013).

Aromatic C=C stretching bands, an indication of benzene-like rings, were also indicated by the peaks at 1402.30, 1417.73, and 1446.66 cm^{-1} in SCBF, SCBB, and Mg-SCBB spectra, respectively, with higher peak intensity in SCBB and Mg-SCBB spectra (Harvey et al., 2012; Saleh et al., 2013; El-Gamal et al., 2017). Bands appeared at 500-700 cm^{-1} may indicate the presence of halide-alkyl vibrational stretching and/or inorganic metal compounds such as of Ca, Mg, or K (Claoston et al., 2014).

Similarities and differences in the characteristic surface functional groups of SCBF and the generated biochars reveal that changes occurred in the molecular structure and surface configuration of the generated biochars leading to the loss of aliphatic, alcohol and
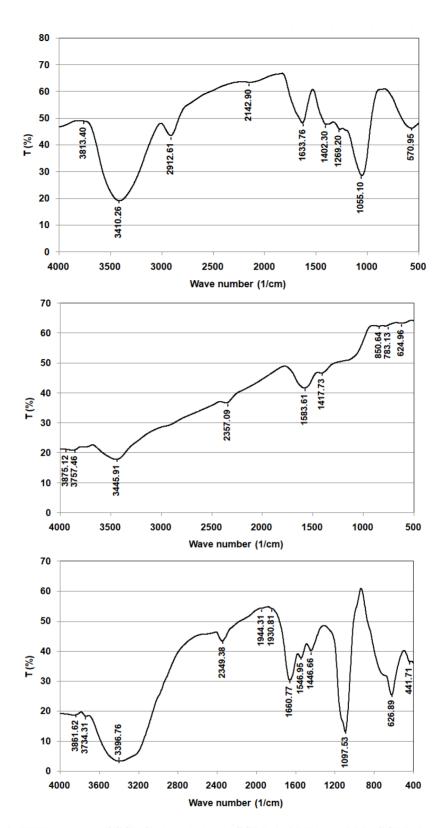
Fig. 2. FTIR spectra of SCB feedstock (top), SCBB (middle), and Mg-SCBB (bottom)
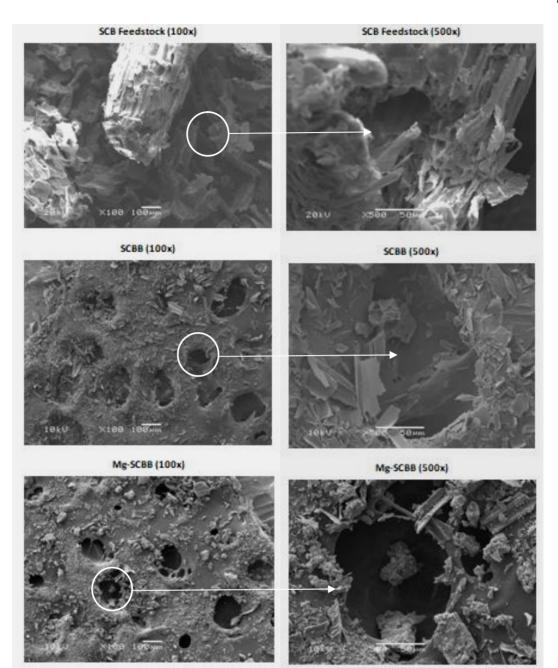
Fig. 3.SEM images of SCB feedstock (top), SCBB (middle), and Mg-SCBB (bottom) at 100x (left) and 500 x (right) magnifications

alkane compound, sugar, and cellulosic and the increase in the aromaticity as temperature increases during pyrolysis (Liu et al., 2015; Carrier et al., 2012; Saleh et al., 2013; El-Gamal et al., 2017).

Microstructure using SEM imaging.

The microstructure of SCBF, SCBB, and Mg-SCBB was investigated by SEM imaging (Fig. 3). It can be observed that SCBF has a complex porous network and that it has fibrous, smooth surfaces in which macropores are dominant. However, pyrolysis at 500 °C led to

coarse surfaces of the generated biochars specially Mg-SCBB and a more porous structure can be seen in the SEM images. More meso- and micropores in the generated SCBB biochar were developed on the account of macropores. Micropores were even increased in Mg-SCBB biochar compared to SCBB. The development of these micropores in Mg-SCBB may explain the higher surface area measured for this modified biochar (Table 2). Due to $MgSO_4$ impregnation, surface coverage with $Mg(OH)_2$ or MgO crystals could be also identified on

Mg-SCBB surfaces compared to SCBB. Changes in the pore configurations of the generated biochars compared with the feedstock are presumably due to the thermal decomposition of cellulose and hemicellulose during the pyrolysis process leaving the cell walls which has higher proportions of lignin compounds. These results are similar to those obtained by Bonelli et al. (2006), Carrier et al. (2012), Harvey et al. (2012), Saleh et al. (2013); Liu et al. (2015), and El-Gamal et al. (2017) who observed similar changes in the surface morphology and size distribution of pores of biochars generated by the pyrolysis of sugarcane bagasse and other agricultural waste materials. These changes were found to be dependent on the type of feedstock, pyrolysis temperature, and the pre- or post-pyrolysis treatments (El-Gamal et al., 2017; Sizmur et al., 2017).

Adsorption kinetics of ammonium and phosphate ions:

Results of adsorption kinetics of ammonium ions (Fig. 4) revealed that sorption of ammonium from aqueous solutions by the tested sorbents was very fast during the first two hours. SCBB and Mg-SCBB were capable of removing ammonium from the aqueous solution at both 1:200 and 1:500 sorbent to solution ratios. For 1:200 ratio and 23 mg/l of initial ammonium concentration, the maximum ammonium removal percent had the order: Zeolite> Mg-SCBB> SCBB> Charcoal (96.41, 80.38, 67.87, and 61.81%,

respectively) and were achieved after 12 h of contact time. However, the ammonium removal percents for these sorbents were very close to each other at 1:500 ratio and they were generally lower than those at 1:200 (72.78, 52.58, 51.13, and 50.19%, for Zeolite, Mg-SCBB, SCBB, and Charcoal, respectively). The developed meso- and micropores in the porous structure, due to modification by $MgSO_4$ impregnation of SCBF, enhanced the efficiency of Mg-SCBB to remove ammonium from solution compared with SCBB and it performed comparably to Zeolite and Charcoal. Similar results were obtained Yao et al. (2013), Fang et al. (2014) and Takaya et al. (2016) who found that pretreatments of biomasses with metal solutions enhanced the efficiency of the generated biochars in removing inorganic ions (NH_4^+, NO_3^-, PO_4-P) from aqueous solutions.

Ammonia volatilization continued during the ammonium adsorption process due to the alkaline conditions of the solution (Fig. 5). Mg-SCBB exhibited the highest cumulative ammonia volatilization. This could be explained by its strong alkaline effect due to MgO hydrolysis compared with the other sorbents (Fig. 6). However, SCBB and Zeolite recorded the least cumulative ammonia volatilization due to their lower solution pH. Cumulative ammonia volatilization for the tested sorbents did not change considerably between the 1:200 and 1:500 ratios.
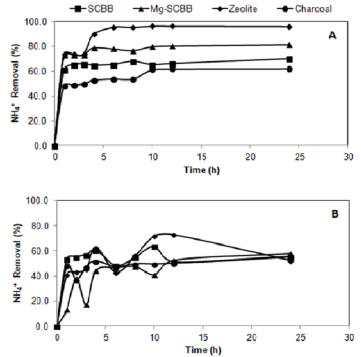

Fig. 4. Percent of NH_4^+ removal from aqueous solutions by different sorbents at A) 1:200, and B) 1:500 sorbent: solution ratios
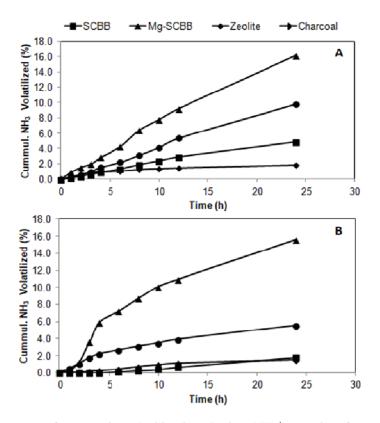
Fig. 5. Cumulative percent of ammonia volatilization during NH_4^+ sorption from aqueous solutions by different sorbents at A) 1:200, and B) 1:500 sorbent: solution ratios
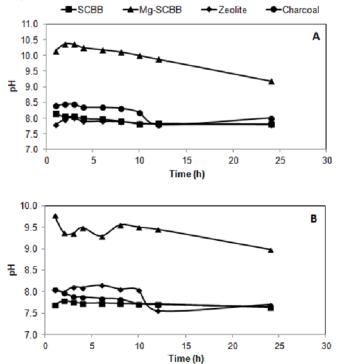

Fig. 6. Changes in pH during NH_4^+ or P removal from aqueous solutions by different sorbents at A) 1:200, and B) 1:500 sorbent: solution ratios
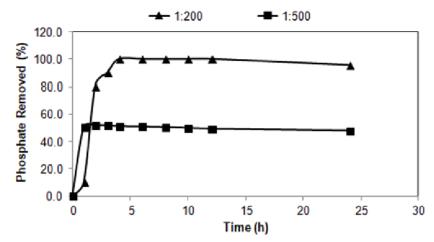
Fig. 7. Percent of phosphate removal from aqueous solutions by Mg-SCBB at 1:200 and 1:500 sorbent: solution ratios

Table 3. Regression parameters of fitting NH_4^+ and P adsorption kinetics data to different linear forms of pseudo-second-order equation

Sorbate/Sorbent	Ratio	Eq.	Slope	Intercept	R^2	Sorbate/Sorbent	Ratio	Slope	Intercept	R^2
NH4/SCBB	1:500	6-1	1.0E-04	1.0E-04	0.997	P/Mg-SCBB	1:200	2.0E-04	2.0E-04	0.991
		6-2	5.0E-05	1.0E-04	0.628			4.0E-04	2.0E-04	0.901
		6-3	-0.5921	7419.6	0.914			-1.1649	4621.6	0.870
		6-4	-1.5431	11682	0.914			-0.7464	3613.7	0.870
NH4/SCBB	1:200	1	3.0E-04	1.0E-04	0.999	NH4/Zeolite	1:500	1.0E-04	1.0E-04	0.997
		2	3.0E-05	3.0E-04	0.682			5.0E-05	1.0E-04	0.629
		3	-0.5865	3466.2	0.763			-0.5918	7418	0.914
		4	-1.3007	4801.1	0.763			-1.544	11687	0.914
NH4/Mg-SCBB	1:500	1	1.0E-04	4.0E-05	1.000	NH4/Zeolite	1:200	2.0E-04	1.0E-04	0.998
		2	1.0E-05	1.0E-04	0.929			9.0E-05	2.0E-04	0.659
		3	-0.5837	8750.6	0.750			-0.8361	4858.5	0.802
		4	-1.2851	12023	0.750			-9.6E-01	4943.5	0.802
NH4/Mg-SCBB	1:200	1	3.0E-04	1.0E-04	0.999	NH4/Charcoal	1:500	1.0E-04	1.0E-04	0.997
		2	3.0E-05	3.0E-04	0.605			4.0E-05	1.0E-04	0.618
		3	-0.6287	4078	0.681			-0.5789	7306.8	0.911
		4	-1.083	4852	0.681			-1.5735	11738	0.911
P/Mg-SCBB	1:500	1	1.0E-04	2.0E-05	0.996	NH4/Charcoal	1:200	4.0E-04	2.0E-04	0.996
		2	1.0E-04	9.0E-05	0.710			3.0E-05	4.0E-04	0.210
		3	-0.8975	10281	0.736			-0.477	2572.8	0.834
		4	-0.8195	9197.2	0.736			-1.7482	4671.9	0.834

The total removal percent of ammonium (adsorbed + volatilized) was calculated for the tested sorbents after 12 h and at 1:200 ratios and it was found to follow the order: Zeolite> Mg-SCBB> SCBB> Charcoal (95.89, 89.59, 70.78 and 67.17%, respectively).

Although adsorption of phosphate from aqueous solutions was not observed at all for Zeolite, Charcoal or SCBB, it was only evident for Mg-SCBB. Maximum removal percent of phosphate by Mg-SCBB was reached after 2 h of contact time (Fig. 7). Phosphate removal was higher at 1:200 than at 1:500 ratios (79.88 and 50.01%, respectively) exhibiting the same kinetic trend at the two ratios. Yao *et al.* (2013) found that Mg-modified biochars were found to have a better ability of phosphate removal from aqueous solutions. They reported that $Mg(OH)_2$ and MgO nanoparticles were developed on the particles' surfaces of Mg-modified biochars which served as the sorption sites for aqueous phosphate.

Fitting the sorption data of ammonium and phosphate kinetics models revealed that the pseudo-second-order equation (Eq. 6) was capable of representing the experimental data.

Table 4. Adsorption kinetics parameters calculated from fitting the linearized form of pseudo-second-order equation (Eq. 6-1)

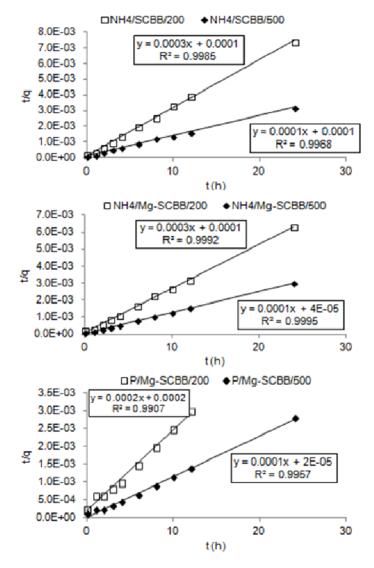| Sorbate/sorbent/ratio	Slope	Intercept	R^2	q_e mg kg^{-1}	k
NH$_4$/SCBB/200	3.0E-04	1.0E-04	0.999	3333.3	9.0E-04
NH$_4$/SCBB/500	1.0E-04	1.0E-04	0.997	10000.0	1.0E-04
NH$_4$/Mg-SCBB/200	3.0E-04	1.0E-04	0.999	3333.3	9.0E-04
NH$_4$/Mg-SCBB/500	1.0E-04	4.0E-05	1.000	10000.0	2.5E-04
NH$_4$/Zeolite/200	2.0E-04	1.0E-04	0.998	5000.0	4.0E-04
NH$_4$/Zeolite/500	1.0E-04	1.0E-04	0.997	10000.0	1.0E-04
NH$_4$/Charcoal/200	4.0E-04	2.0E-04	0.996	2500.0	8.0E-04
NH$_4$/Charcoal/500	1.0E-04	1.0E-04	0.997	10000.0	1.0E-04
P/Mg-SCBB/200	2.0E-04	2.0E-04	0.991	5000.0	2.0E-04
P/Mg-SCBB/500	1.0E-04	2.0E-05	0.996	10000.0	5.0E-04

Fig. 8.Fitting data of NH$_4^+$ and P adsorption by SCBB and Mg-SCBB to the linear form Eq. 6-1 of the pseudo-second-order kinetic equation
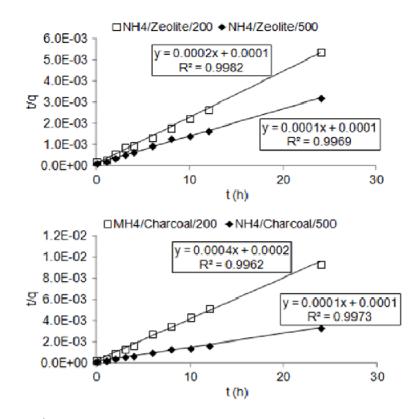
Fig. 9.Fitting data of NH$_4^+$ and P adsorption by Zeolite and Charcoal to the linear form Eq. 6-1 of the pseudo-second-order kinetic equation
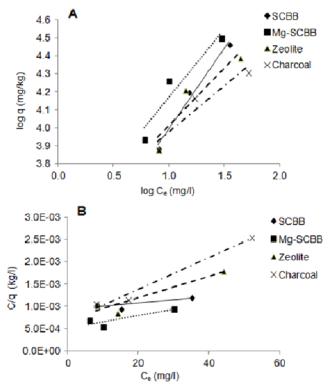

Fig. 10. Fitting data of NH$_4^+$ adsorption on the tested sorbents to A) Freundlich, and B) Langmuir models

Table 5. Calculated parameters of Freundlich model from the corresponding linear regressions

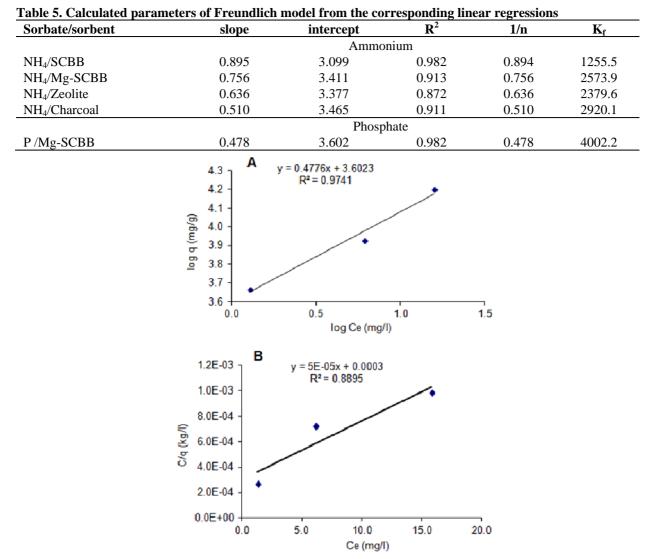| Sorbate/sorbent	slope	intercept	R^2	1/n	K_f
Ammonium					
NH$_4$/SCBB	0.895	3.099	0.982	0.894	1255.5
NH$_4$/Mg-SCBB	0.756	3.411	0.913	0.756	2573.9
NH$_4$/Zeolite	0.636	3.377	0.872	0.636	2379.6
NH$_4$/Charcoal	0.510	3.465	0.911	0.510	2920.1
Phosphate					
P /Mg-SCBB	0.478	3.602	0.982	0.478	4002.2

Fig. 11. Fitting data of P adsorption on Mg-SCBB to A) Freundlich, and B) Langmuir models

Regression parameters of fitting ammonium and phosphate adsorption data are listed in Table (3). Plotting the values of t/q *vs.* t had the highest determination coefficient (R^2) of the linear regression plots for all the tested sorbents and ratios (Fig. 8 and 9). Therefore, the linearized form Eq. (6-1) of the pseudo-second-order equation was the best fit. This may suggest the intraparticle diffusion controlled adsorption of ammonium and phosphate on the tested biochars (Ghasemi *et al.*, 2013; Plazinski *et al.*, 2013; Zhang *et al.*, 2015). Parameters of adsorption kinetics (q$_e$ and k) were then calculated using the obtained slope and intercepts of Eq. (6-1). Generally, the adsorption capacity of ammonium from the aqueous solutions by SCBB and Mg-SCBB were similar and it was higher at 1:500 than at 1:200 (10000 and 3333.3 mg NH$_4^+$ kg^{-1}, respectively). The same trend of q$_e$ was found for phosphate adsorption by Mg-SCBB which recorded 5000 and 10000 mg PO$_4$ kg^{-1} at 1:200 and 1:500, respectively.

Adsorption isotherms:

Data of ammonium adsorption by the tested sorbents at different concentrations showed that adsorption of ammonium increases with increasing its initial concentration in the aqueous solution for all sorbents. Fitting these data to different isotherm models revealed that Freundlich isotherm model was the best fit model (highest R^2) to describe the experimental data (Fig. 10) followed by Langmuir model (R^2 from 0.624 to 871). The parameters of Freundlich model were calculated from the regression equations obtained (Table 5). The calculated parameters may indicate that adsorption capacity (K_f) of sorbents for ammonium followed the order: Charcoal> Mg-SCBB> Zeolite> SCBB (Table 5). However, the intensity parameter (1/n) had the range

from 0.510 to 0.894 and followed the order: SCBB> Mg-SCBB> Zeolite> Charcoal. The calculated n values ranged from 1.96 to 1.12 (between 1 and 10). This may indicate the favorable adsorption of ammonium by the all tested sorbents (Hafshejani et al., 2016).

Isotherms of phosphate adsorption by Mg-SCBB (Fig. 11) confirm that adsorption of phosphate on Mg-SCBB was affected by phosphate concentration. These data were better fitted to the Freundlich model than the Langmuir model (R^2: 0.97 and 0.89, respectively). The calculated phosphate adsorption capacity and intensity of this sorbent were 4002.2 and 0.478 mg kg^{-1}, respectively. The calculated value of n (2.09) may indicate the favorable adsorption of phosphate ion on Mg-SCBB. These results are consistent with those obtained by Shwantes *et al*. (2015). On the other hand, Trazzi *et al.* (2016) found that Langmuir model gave higher R^2 than Freundlich model for adsorption of phosphate ions on sugarcane bagasse biochar.

Accordingly, SCBB and Mg-SCBB biochars proved to have the ability to adsorb ammonium from aqueous solutions compared with the well-known sorbents Zeolite and Charcoal. In addition, Mg-SCBB was the only sorbent capable of removing both ammonium and phosphate from these solutions. Therefore, Mg-SCBB can be used for an efficient dual removal of these two ions from aqueous solutions.

CONCLUSIONS

Pyrolysis of sugarcane bagasse at 500 ℃ under oxygen-limited condition produced a biochar which is capable of efficiently removing ammonium ions from aqueous solutions and it was comparable to commercial Charcoal and Zeolite sorbents. Pre-pyrolysis MgSO$_4$ impregnation of bagasse feedstock produced modified biochar with a dual capability of removing ammonium and phosphate ions from aqueous solutions. Changes in the physical and chemical properties occurred in the generated biochars as compared to the feedstock. Analysis of FTIR bands and SEM investigations revealed that surface chemical functional groups and meso- and micropores were developed due to pyrolysis. Adsorption kinetics data of both ammonium and phosphate ions on the tested sorbents were best described by the linearized form of the second-pseudo-order equation indicating the intraparticle diffusion controlled adsorption of ammonium and phosphate. Ammonium and phosphate adsorption isotherms were best fitted to the Freundlich model and revealed that the adsorption of these ions was favorable by the generated biochars. The Mg-modified sugarcane bagasse biochar can be considered as a promising sorbent for dual removal of ammonium and phosphate ions from aqueous solutions. Further research is needed to investigate the influences of various physical and chemical factors on the efficacy of this biochar in remediating contaminated wastewater.

REFERENCES

Agegnehu, G., A.K. Srivastavab, and M. I. Bird. 2017.The role of biochar and biochar-compost in improving soil quality and crop performance: A review. Applied Soil Ecol. 119:156–170.

Beesley, L., E. M. Jiménez, and J. L. G. Eyles. 2010. Effects of biochar and green waste compost amendments on mobility, bioavailability, and toxicity of inorganic and organic contaminants in a multi-element polluted soil. Environ. Pollut. 158: 2282–2287.

Bonelli, P. R., M. E. Ramos, E. L. Buonomo, and A. L. Cukierman. 2006. Potentialities of the biochar generated from raw and acid Pre-Treated sugarcane agricultural wastes. 8thAsia-Pacific International Symposium on Combustion and Energy Utilization. October 10-12, 2006, Sochi, Russian Federation.

Cai, R., X. Wang, X. Ji, B. Peng, C. Tan, and X. Huang. 2017. Phosphate reclaim from simulated and real eutrophic water by magnetic biochar derived from water hyacinth. J. Environ. Manage. 187: 212–219.

Carey, D. E., P. J. McNamara, and D. Zitomer. 2015. Biochar from Pyrolysis of Biosolids for Nutrient Adsorption and Turfgrass Cultivation. Water Environ. Res. 87: 2098-2106.

Carrier, M., A. G. Hardieb, U. Urasa, J. Gorgensa, and J. Knoetze. 2012. Production of char from vacuum pyrolysis of South-African sugar cane bagasse and its characterization as activated carbon and biochar. J. Anal. Appl. Pyrolysis 96: 24–32.

Cha, J. S., S. H. Park, S. Jung, C. Ryu, J. Jeon, M. Shin, and Y. Park. 2016. Production and utilization of biochar: A review. J. Industr. Engineer. Chem. 40: 1–15.

Claoston, N., A. Samsuri, M. A. Husni, and M. M. Amran. 2014. Effects of Pyrolysis Temperature on the Physicochemical Properties of Empty Fruit Bunch and Rice Husk Biochars. Waste Manage. Res. 32: 331–339.

Conley, D.J., H.W. Paerl, R.W. Howarth, D.F. Boesch, S.P. Seitzinger, K.E. Havens, C. Lancelot, and G.E. Likens. 2009. Controlling eutrophication: nitrogen and phosphorus. Sci. 323:1014–1015.

Daffalla, S. B., H. Mukhtar and M. S. Shaharun. 2010. Characterization of Adsorbent Developed from Rice Husk: Effect of Surface Functional Group on Phenol Adsorption. J. Applied Sci. 10: 1060-1067.

De Jesus, J.H.F., G. da C. Cunha, E.M.C. Cardoso, A.S. Mangrich, and L.P.C. Romao. 2017. Evaluation of waste biomasses and their biochars for removal of polycyclic aromatic hydrocarbons. J. Environ. Manage. 200: 186-195.

Ding, W., X. Dong, I. M. Ime, B. Gao, and L. Q. Mad. 2014. Pyrolytic temperatures impact lead sorption mechanisms by bagasse biochars. Chemosphere 105: 68–74.

Dunnivant, F. and E. Anders (eds.). 2006. A basic introduction to pollutant fate and transport. Wiley Interscience, John Wiley, and Sons, Inco., Publication. Hoboken, New Jersey, USA.

El-Gamal, E. H., M. Saleh, I. Elsokkary, M. Rashad, M. M. Abd El-Latif. 2017. Comparison between Properties of Biochar Produced by Traditional and Controlled Pyrolysis.Alex. Sci. Exch. J. 38:412-425.

Fang, Ci, T. Zhang, P. Li, R. Jiang, and Y. Wang. 2014. Application of Magnesium Modified Corn Biochar for Phosphorus Removal and Recovery from Swine Wastewater Int. J. Environ. Res. Public Health 11: 9217-9237

FAS-USDA, 2017. Egypt, Sugar Annual Report 2017: Egypt's Government Increases the Supply Price for Sugar Cane and Beets Ceding to Farmers' Demands. USDA Foreign Agriculture Service Report. Issued on 18/4/2017. Accessed on 12/9/2017. https://www.fas.usda.gov/data/egypt-sugar-annual-2

Gaskin, J. W., C. Steiner, K. Harris, K. C. Das, and B. Bibens. 2008. Effect of Low- Temperature Pyrolysis Conditions on Biochar for Agricultural Use. Am. Soc. Agric. Biol. Engin. 51: 2061-2069.

Ghasemi, N., P. Tamri, A. Khademi, N. S. nezhad, and S. R. W. Alwi. 2013. Linearized equations of pseudo second-order kinetic for the adsorption of Pb (II) on Pistacia Atlantica shells. IERI Procedia 5: 232- 237.

Hafshejani, L. D., A. Hooshmand, A. A. Naseri, A. S. Mohammadi, F. Abbasi, and A. Bhatnagar. 2016. Removal of nitrate from aqueous solution by modified sugarcane bagasse biochar. Ecol. Engin. 95:101–111.

Harvey, R. O., B. E. Herbert, L. J. Kuo, P. Louchouarn, 2012. Generalized two-dimensional perturbation correlation infrared spectroscopy reveals mechanisms for the development of surface charge and recalcitrance in plant-derived biochars. Environ. Sci. Technol., 46: 10641-10650.

Ho, Y.S. 2006. Second-order kinetic model for the sorption of cadmium onto tree fern: A comparison of linear and non-linear methods. Water Res. 40: 119–125.

Ho, Y.S. and G. McKay. 1999. Pseudo-second order model for sorption processes. Process. Biochem. 34: 451–465.

Huang, Y., P. Chiueh, C. Shih, S. Lo, L. Sun, Y. Zhong, and C. Qiu. 2015. Microwave pyrolysis of rice straw to produce biochar as an adsorbent for CO_2 capture. Energy 84: 75-82.

Hugo, T. J. 2010. Pyrolysis of sugarcane bagasse. M. Sc. Thesis. Department of Process Engineering, University of Stellenbosch. South Africa. p 217.

Inyang, M., B. Gao, P. Pullammanappallil, W. Ding, and A. R. Zimmerman. 2010. Biochar from anaerobically digested sugarcane bagasse Bioresour. Technol. 101: 8868-8872.

Jeong C. Y., S. K. Dodla, and J. J. Wang. 2016. Fundamental and molecular composition characteristics of biochars produced from sugarcane and rice crop residues and by-products. Chemosphere 142: 4–13.

Jiang, Y.P., X.F. Yang, Z.H. Zhang, C.H. Chen, and L.J. Wang. 2013. Progress of the effect of biomass charcoal on soil environment and crop growth. J. Zhejiang Agric. Sci. 25:410–415.

Jindo, K., H. Mizumoto, Y. Sawada, M. A. Sanchez-Monedero, and T. Sonoki. 2014. Physical and chemical characterization of biochars derived from different agricultural residues. Biogeosciences. 11: 6613–6621.

Kaewprasit, C., E. Hequet, N. Abidi, J. P. Gourlot. 1998. Application of methylene blue adsorption to cotton fiber specific surface area measurement: part I. Methodology. J. Cotton Sci. 2, 164–173.

Keeney, D. R. and D. W. Nelson. 1982. Nitrogen – Inorganic forms. In A. L. Page (ed.), Methods of Soil Analysis, Part 2. pp. 643-698. Am. Soc. Agron., Soil Sci. Soc. Am. Madison, Wis. USA.

Li, H., X. Dong, E. B. da Silva, L. M. de Oliveira, Y. Chen, and L. Q. Ma. 2017. Mechanisms of metal sorption by biochars: Biochar characteristics and modifications Chemosphere 178: 466-478.

Li, J., J. Dai, G. Liu, H. Zhang, Z. Gao, J. Fu, Y. He, and Y. Huang. 2016. Biochar from microwave pyrolysis of biomass: A review. Biomass and Bioenergy 94: 228-244.

Liu, F., J. Zuo, T. Chi, P. Wang, and B. Yang. 2015. Removing phosphorus from aqueous solutions by using iron-modified corn straw biochar. Front. Environ. Sci. Engin. 2015, 9(6): 1066–1075.

Luo, L., C. Xu, Z. Chen, and S. Zhang. 2015. Properties of biomass-derived biochars: Combined effects of operating conditions and biomass types. Bioresour. Technol. 192: 83–89.

Murphy, J. and J. P. Riley. 1962. A modified single solution method for the determination of phosphates in natural waters. Anal. Chem. Acta 27: 31–36.

Noraini, M. N., E. C. Abdullah, R. Othman, and N.M. Mubarak. 2016. Single-route synthesis of magnetic biochar from sugarcane bagasse by microwave-assisted pyrolysis. Materials Letters 184: 315–319.

Pan, G.X., A.F. Zhang, and J.W. Zou. 2010. Biochar from agro-byproducts used as an amendment to croplands: an option for low carbon agriculture. J. Ecol. Rural Environ. 26: 394–400.

Plazinski, W., J. Dziuba, and W. Rudzinski. 2013. Modeling of sorption kinetics: the pseudo-second-order equation and the sorbate intraparticle diffusivity. Adsorption 19:1055-1064.

Qiu, Y., Z. Zheng, Z. Zhou, and G.D. Sheng. 2009. Effectiveness and mechanisms of dye adsorption on a straw-based biochar. Bioresour. Technol. 100: 5348–5351.

Saleh, M. E., A. A. El-Refaey and A. H. Mahmoud. 2016. Effectiveness of Sunflower Seed Husk Biochar for Removing Copper Ions from Wastewater: a Comparative Study. Soil Water Res. 11: 53–63.

Saleh, M. E., A. H. Mahmoud and M. Rashad. 2012. Peanut Biochar as a Stable Adsorbent for Removing NH4-N from Wastewater: A Preliminary Study. Advances in Environ. Biol. 6: 2170-2176.

Saleh, M. E., A. H. Mahmoud, and M. Rashad. 2013. Biochar Usage as a cost-effective bio-sorbent for removing NH$_4$-N from wastewater. The international conference the Global Climate Change, Biodiversity and Sustainability: Challenges and Opportunities in Arab MENA region and EuroMed. 15-18 April 2013 Alexandria, Egypt.

Samsuri A.W., F. Sadegh-Zadeh, and B. J. Seh-Bardan. 2014. Characterization of biochars produced from oil palm and rice husks and their adsorption capacities for heavy metals. Int. J. Environ. Sci. Technol. 11: 967–976.

Schwantes. D., A. C. Gonçalves Jr., D. C. Schons, T. G. Veiga, R. C. Diel, and V. Schwantes. 2015. Nitrate Adsorption using Sugar Cane Bagasse Physicochemically Changed. J. Agric. Environ. Sci. 4: 51-59.

Sizmur T., T. Fresno, G. Akgül, H. Frost, and E. Moreno-Jiménez. 2017. Biochar modification to enhance sorption of inorganics from water. Bioresour. Technol. (*in press*)

Strock, J., A. Ranaivoson, G. Feyereisen, K. Spokas, D. Mulla, and M. Roser. 2017. Nutrient removal in agricultural drainage ditches. Final Report for State of Minnesota Project Contract #63906, p 99.

Takaya, C. A., L. A. Fletcher, S. Singh, U.C. Okwuosa, and A. B. Ross. 2016. Recovery of phosphate with chemically modified biochars. J. Environ. Chem. Engineer. 4:1156-1165.

Tan, Z., C. S. K. Lin, X. Ji, and T. J. Rainey. 2017. Returning biochar to fields: A review. Applied Soil Ecol. 116:1–11.

Teixid?, M., J. J. Pignatello, J. L. Beltr?n, M. Granados, and J. Peccia. 2011. Speciation of the ionizable antibiotic sulfamethazine on black carbon (biochar). Environ. Sci. Technol. 45:10020–27.

Trazzi, P. A., J. J. Leahy, M. H. B. Hayes, and W. Kwapinski. 2016. Adsorption and desorption of phosphate on biochars. J. Environ. Chem. Engin. 4: 37–46.

Ulyett, J., R. Sakrabani, M. Kibblewhite, and M. Hann. 2014. Impact of biochar addition on water retention, nitrification and carbon dioxide evolution from two sandy loam soils. Europ. J. Soil Sci. 65:96–104.

Weber, W., and J. Morris. 1963. Kinetics of adsorption on carbon from solution. J. Sanit. Eng. Div. Am. Soc. Civ. Eng. 89: 31–60.

WHO. 2017. Don't pollute my future! The impact of the environment on children's health. World Health Organization. Geneva, License: CC BY-NC-SA 3.0 IGO. 130.

Xu, R.K., S.C. Xiao, J.H. Yuan, and A.Z. Zhao. 2011. Adsorption of methyl violet from aqueous solutions by the biochar derived from crop residues. Bioresour. Technol. 102: 10293–298.

Yao, Y., B. Gao, J. Chen, M. Zhang, M. Inyang, Y. Li, A. Alva, L. Yang. 2013. Engineered carbon (biochar) prepared by direct pyrolysis of Mg-accumulated tomato tissues: characterization and phosphate removal potential. Bioresour. Technol. 138: 8–13.

Zhang, L., H. A. Lo?iciga, M. Xu, C. Du and Y. Du. 2015. Kinetics and Mechanisms of Phosphorus Adsorption in Soils from Diverse Ecological Zones in the Source Area of a Drinking-Water Reservoir Int. J. Environ. Res. Public Health 12: 14312-14326

Zhang, Z.H., Z.H. Lin, and Y.Q. Fu. 2010. The state of applications of biochar in agriculture. J. Anhui Agric. Sci. 38:11880–11882.

Zheng, W., M. Guo, T. Chow, D.N. Bennett, and N. Rajagopalan. 2010. Sorption properties of greenwaste biochar for two triazine pesticides. J. Hazard. Mater. 181: 121–126.

الملخص العربي

استخدام مخلفات عصر قصب السكر المعدلة بالمغنسيوم في الإزالة المزدوجة لأيونات الأمونيوم والفوسفات من المحاليل المائية

ماهر السيد صالح ، رمزي مرسي رزق هـدية

إن استغلال المخلفات الزراعيـة فـي إنتاج مـواد إدمصاص رخيصة ذات كفاءة عالية لإزالة الملوثـات مـن المياه العادمة يعتبر من التحديات البيئية المعاصـرة. وفـي مصر، تنتج عملية عصر قصب السكر كميت هائلة مـن مصاصة قصب السكر (SCBF) بكميات هائلة كمواد عادمة. وتهدف هذه الدراسة إلى بحث تأثير التعديل الكيميائي على خواص الفحم الحيوي لمصاصة قصب السكر ، وتقويم كفاءة هذا الفحم في إزالة كل من أيونات الأمونيوم والفوسفات من المحاليل المائية الإصطناعية.

تم إنتاج فحم مصاصة القصب الخـام (SCBB) وفحـم مصاصة القصب المعدلة بالمغنسيوم (Mg-SCBB) بطريقـة التحلل الحراري عند درجة حرارة ٥٠٠ ºم تحت ظـروف محدودة من الأوكسجين لمصاصة القصب الخام والمخصبة بكبريتات المغنسيوم، على التـوالي. وقـد دلـت تحاليـل منحنيــات FTIR، وفحوصــات صــور مسـح الســطح بالميكروسكوب الإلكتروني SEM، وكذلك بعض الخـواص الفزيائية والكيميائية لنوعي الفحم الناتجين على ظهور العديد من المجاميع الكيميائية السطحية، وتكوين المسام المتوسطة والدقيقة، وزيادة مساحة الأسطح، وكـذلك إرتفـاع السـعة التبادلية الكاتيونية بالمقارنة بالمادة الأولية (SCBF).

وقد أظهرا نوعي الفحم Mg-SCBB, SCBB اللذان تـم إنتاجهما ميولا عالية وقدرة على إمتصاص أيون الأمونيوم من المحاليل المائية مقارنـة بـالفحم الحجـري Charcoal والزيولايت Zeolite. كما وجد أن الفحم Mg-SCBB (الناتج من تخصيب مصاصة القصب بالمغنسيوم) هو الوحيد القادر على إزالة أيونات الفوسفات من المحاليل المائيـة. وكـان مقدار إزالة أيونات الأمونيوم والفوسفات عند نسـبة مـادة الإدمصاص إلى المحلول ٢٠٠:١ بشكل عـام أعلـى مـن النسبة ٥٠٠:١ عند نفس التركيزات. وقد ثبت حدوث تطاير طفيف لغاز الأمونيوم من المحاليل أثناء عملية الإدمصاص نتيجة إرتفاع رقم الــ pH لمعلقـات مـواد الإدمصـاص المختبرة مع المحاليل.

ووجد أن نتائج حركية إدمصاص Adsorption Kinetics أيونات الأمونيوم والفوسفات تنطبق مـع معادلـة شـبيهة الدرجة الثانية Pseudo-Second-Order، مما يدل علـى أن ميكانيكية الإنتشار خلال حبيبات مـادة الإدمصاص هـي الخطوة المتحكمة في عملية الإدمصاص. كما ثبت أن نتائج منحنيات الإدمصـاص عنـد درجـات حـرارة متسـاوية Adsorption Isotherms إنطبقت بصورة أفضل مع نمـوذج فرويندليخ الرياضي Freundlich Model. وكانت قيم معامل الشدة لنموذج فرويندليخ (n) تتراوح بين ٠.٤٧٨ و ٠.٨٩٤ مما يدل علـى أفضـلية إدمصـاص أيونـات الأمونيـوم والفوسفات بواسطة مواد الإدمصاص المختبرة. وكانت سعة الفحم الحيوي Mg-SCBB لإدمصاص الأمونيـوم هـي ٢٥٧٣.٩ مجم/كجم، وللفوسفات هي ٤٠٠٢.٢ مجم/كجـم. ويمكن القول بأن الفحم الحيوي المنتج من مصاصة القصب المخصبة بكبريتات المغنسيوم (Mg-SCBB) يمكن أن يمثل مادة إدمصاص واعدة، رخيصة الـثمن، وعاليـة الكفـاءة للمعالجة الثنائية للمياه العادمة الملوثة بأيونـات الأمونيـوم والفوسفات.